Title

Energy and electron drift time measurements in a pixel CCI TlBr detector with 1.3 MeV prompt-gammas

Journal

Physics in Medicine and Biology, 66(4)

ISSN

0031-9155

Authors

Ariño-Estrada, Gerard
Kim, Hadong
Du, Junwei
et al.

Publication Date

2021-02-21

DOI

10.1088/1361-6560/abd419

Peer reviewed

HHS Public Access

Author manuscript

Phys Med Biol. Author manuscript; available in PMC 2022 April 20.

Published in final edited form as:

Phys Med Biol. ; 66(4): 044001. doi:10.1088/1361-6560/abd419.

Energy and electron drift time measurements in a pixel CCI TlBr detector with 1.3 MeV prompt-gammas

Gerard Ariño-Estrada[1,*], **Hadong Kim**[2], **Junwei Du**[1], **Leonard J Cirignano**[2], **Kanai S Shah**[2], **Simon R Cherry**[1]

[1]Department of Biomedical Engineering, University of California Davis, Davis, CA 95616, United States of America

[2]Radiation Monitoring Devices, Inc., Watertown, MA 02472, United States of America

Abstract

Assessing the position of the Bragg peak (BP) in hadron radiotherapy utilizing prompt-gamma imaging (PGI) presents many challenges in terms of detector physics. Gamma detectors with the capability of extracting the best energy, timing, and spatial information from each gamma interaction, as well as with high detection efficiency and count rate performance, are needed for this application. In this work we present the characterization of a pixel Čerenkov charge induction (CCI) thallium bromide (TlBr) detector in terms of energy and and electron drift time for its potential use in PGI. The CCI TlBr detector had dimensions of $4 \times 4 \times 5$ mm^3 and one of its electrodes was segmented in pixels with 1.7 mm pitch. A silicon photomultiplier (SiPM) was optically coupled to one of the faces of the TlBr slab to read out the Čerenkov light promptly emitted after the interaction of a gamma ray. The detector was operated stand-alone and the 1.275 prompt gammas from a ^{22}Na radioactive source were used for the study. The electron drift time was obtained by combining the Čerenkov and charge induction signals and then used as a measure of the depth of interaction. The electron mobility in TlBr was estimated as ~27 cm^2 V^{-1} s^{-1}. Energy resolutions between 3.4% and 4.0% at 1.275 MeV were obtained after depth-correction. These values improved to 3.0%–3.3% when events with drift times of 3–6 μs were selected. These results show the potential of pixel CCI TlBr detectors to resolve gamma interactions in the detector with mm-like accuracy in 3D and with excellent energy resolution. Previous studies with CCI TlBr devices have shown a timing resolution of <400 ps full width at half maximum when detecting 511 keV gamma rays, therefore, the timing accuracy is expected to improve with the increased energy of the gamma rays in PGI. While other important detector characteristics such as count rate capability remain to be studied, results from this work combined with other preliminary data show pixel CCI detectors can simultaneously provide excellent energy, timing, and spatial resolution performance and are a very promising option for PGI in hadron therapy.

Keywords

TlBr; proton therapy; prompt gamma imaging; Cerenkov charge induction detectors; electron drift time in TlBr; energy depth-correction in TlBr

[*]Author to whom any correspondence should be addressed: garino@ucdavis.edu.

1. Introduction

Cancer radiotherapy using protons or ions is an attractive treatment option as it has the potential to better preserve healthy tissue surrounding the tumor compared to radiation with photons or electrons (Durante et al 2017). The main outstanding challenge in hadron therapy is to estimate the range of the protons or ions in the patient's body to assess if the dose is properly delivered to the tumor. Prompt-gamma imaging (PGI) aims to estimate the Bragg peak (BP) position by using the prompt-gammas emitted by the excited states of carbon and oxygen atoms, which are predominantly produced at the end of the proton or ion range. However, PGI poses several intrinsic challenges such as the detection of prompt-gammas themselves, given their energies range between 1 and 6 MeV, and limited available counts. Moreover, a fast and very precise localization of the BP would be desired to allow for effective adjustment of the treatment settings.

Some of the methods proposed for proton range verification (PRV) using PGI are prompt gamma-ray spectroscopy (PGS) (Hueso-González et al 2018), prompt gamma-ray timing (PGT) (Golnik et al 2014), or the Compton camera approach (CC) (Krimmer et al 2015, Llosá et al 2016). Each of these methods poses different performance trade-offs and require different detector features such as timing resolution (PGT), 3D detector event localization (CC), or high energy resolution (CC and PGS). Pausch et al (2018) suggested the aforementioned methods might be combined to improve the imaging performance, however, that approach requires a radiation detector with simultaneously high performance in energy, timing, and spatial resolution, as well as high detection efficiency and count rate capability.

Čerenkov charge induction (CCI) detectors have the potential to provide such performance. CCI detectors consist of a semiconductor material that is simultaneously a Čerenkov emitter, and combines the charge induction readout of semiconductor detectors with the detection of Čerenkov light. The performance of a CCI detector made of thallium bromide (TlBr) with strip electrodes was reported in Ariño-Estrada et al (2019). That study showed the feasibility of operating the charge induction and Čerenkov readouts simultaneously and reported a timing resolution below 400 ps full width at half maximum (FWHM). Moreover, TlBr has high atomic numbers and density when compared to detector materials commonly used in (or proposed for) positron emission computed tomography (PET) such as lutetium oxyorthosilicate (LSO), bismuth germanate (BGO), lanthanum bromide ($LaBr_3$) or cadmium-(zinc)-telluride (Cd(Zn)Te) (Ariño-Estrada et al 2018b). Table 1 shows the attenuation length of such materials, compared with TlBr, for energies between 1 and 6 MeV.

This work reports on the performance of a CCI TlBr detector with pixel electrodes. The energy resolution and the estimation of the electron drift time were evaluated. Semiconductor detectors require a depth-correction of the energy resolution to minimize the effect of trapping of their charge carriers (Lachish 2001). Two main approaches are commonly used: the cathode-to-anode ratio (CAR) method (He et al 1999) and the evaluation of the drift time based on the cathode signal (Cai and Meng 2013). Reading the cathode signal is required in both methods. This study evaluated the feasibility of using the

Čerenkov signal to determine the start of the electron drift, and the pixel signal for the stop, without reading out the cathode. As the Čerenkov signal is very fast, this method could allow a depth-correction to be applied for multiple interactions occurring in several pixels within a short time and to obtain high counting rates independently of the cathode area, and therefore bulk size.

A complete validation of gamma detectors for PGI also requires a study of other aspects such as their dead time, maximum count rate capability, or their behavior under strong background fluxes. This study focuses on the detector performance at 1.275 MeV so that it can be carried out in a benchtop setting, and with minimization of the contribution of undesired noise sources. This work aims to be a stepping stone towards future upgrades of pixel CCI detectors for the detection of gammas with higher energies in a cyclotron environment.

2. Materials and methods

2.1. Detector

The pixel CCI TlBr detector used for this study had dimensions of 4 mm × 4 mm × 5 mm and was manufactured by Radiation Monitoring Devices, Inc. (RMD, Watertown, MA). TlBr was grown by the traveling molten zone (TMZ) method (Churilov et al 2008). The sample was cut from a larger ingot and then lapped, polished and chemically etched. An electrode layer was deposited on two opposing 4 mm × 5 mm faces. The cathode was monolithic and the electrode was segmented into 4 pixels arranged in a 2 × 2 fashion with 1.7 mm pixel pitch and the surrounding electrodes shorted to act as a guard ring (GR), figure 1 (left). The detector was then mounted on a small printed circuit board (PCB) standing on one of its 4 mm × 4 mm faces, figure 1 (right). The four pixels and GR were connected to the PCB. All the 4 mm × 5 mm faces from the detector were wrapped with Teflon. A silicon photomultiplier (SiPM) S14160-6050HS (Hamamatsu Photonics K.K., Hamamatsu, Japan), with a total surface of 6 mm × 6 mm was coupled to the top 4 mm × 4 mm of the TlBr slab using optical grease (BC-630, Saint-Gobain, Courbevoie, France). The TlBr was biased at −600 V and the SiPM at 41.0 V. The detector was operated at room temperature.

2.2. Readout

Figure 2 depicts the readout setup. Each of the four pixels were connected to a charge sensitive preamplifier (preamp) CR110 (Cremat Inc., Watertown, OR). The GR segments of the anode were shorted and were also connected to one CR110 preamplifier to keep the whole GR at the same potential as the pixels. The output of each preamplifier was split into two: one was connected to the spectroscopy amplifier N1068GE (CAEN, Via Reggio, Italy) and the other was recorded with a 5740D (CAEN) digitizer. The shaping time of the N1068GE was set to 8 μs. The shaped output of each pixel was recorded with the digitizer. The N1068GE also offered a timing section based on constant fraction discriminators (CFD) with auto walk compensation and an independent trigger signal for each input. The four triggers corresponding to the four pixels were combined using an OR logic implemented in the same module. The SiPM signal was coupled to the KETEK (KETEK GmbH, München, Germany) test board, then to a NIM linear amplifier module, and was also recorded with the

5740D digitizer. Nine signals were recorded per event (4 preamp signals, 4 shaped signals, and 1 SiPM signal) at a sampling rate of 62.5 MS s^{-1} and a record length of 4000 samples (64 μs). A ^{22}Na source with an activity of 740 kBq (20 μCi) was placed approximately 1 cm from the detector and the trigger threshold was set to approximately 700 keV to reject 511 keV gammas and detect only 1.275 MeV prompt-gammas.

2.3. Data analysis

The energy deposited on each pixel was measured as the maximum amplitude of the shaped signal on each pixel. The pixel with maximum energy in each event was considered the trigger pixel. The start and end of the electron drift were obtained from the SiPM and preamp signals, respectively. Figure 3 shows a representative event to illustrate the process. The SiPM signal was differentiated. The digitizer trigger position was set before the 1000th sample point and, therefore, the Čerenkov signal corresponding to the start time, if registered, had to be within those 1000 samples. The position of the maximum value of the SiPM differentiated waveform among the first 1000 sample points was taken as the start of the electron drift. The amplitude of the differentiated signal at that point was taken as the Čerenkov amplitude.

The end of the electron drift time was measured as follows. The preamplifier signal of the trigger pixel was filtered using a Butterworth filter (Butterworth 1930) of order 3 and a critical frequency of 0.05 times the digitizer sampling rate, to eliminate the high-frequency noise. This filter was implemented in python3 using the scipy.signal.butter method. The filtered signal was differentiated. Starting from the maximum point of the differentiated curve, points with increasing time index were evaluated and the point equal or immediately before one fifth of the maximum was taken as the end of the electron drift.

Sample points of each waveform were separated by 16 ns. The error in the drift time evaluation was estimated to be a few samples and approximately of the order of 80–100 ns. The maximum drift time for an electron in TlBr with the thickness of this device (4 mm) and bias voltage applied (600 V total) was expected to be of the order of 10 μs, hence the precision of this method was considered sufficient for the purpose of this work.

3. Results

3.1. Čerenkov measurements

Figure 4 shows the spectroscopy of Čerenkov signals measured with the SiPM. The distribution shows six peaks spread fairly homogeneously, which suggests they correspond to an increasing integer number of detected Čerenkov photons. Figure 5 shows the 2D histograms of Čerenkov amplitude versus electron drift time for events triggered by each pixel. Datasets in all pixels showed the same behavior. The peaks from figure 4 showed as horizontal bands. All the bands except for the one with lowest intensity, centered at ~120 analog-to-digitizer converted counts, extended for drift times up to ~ 10 μs. This result suggested a fraction of events in the first peak were due to a misidentification of a dark count as the start of the electron drift time. Based on this measurement, the mobility of electrons in this TlBr device was estimated to be ~27 ± 3 cm^2 s^{-1} V^{-1}.

3.2. Energy measurements

Figure 6 shows the 2D histograms of the raw energy versus electron drift time estimation for each pixel. The photopeak and K-edge escape peak bands were observed for all pixels with drift times between 1 and 9 μs. The position of the 1.275 MeV photopeak as a function of drift time (in 1 μs increments between 1 and 9 μs) for each pixel was used to apply a depth-correction to the raw energy measurements. Linear interpolation between drift time points was used. Events with drift times smaller than 1 μs or greater than 9 μs were rejected.

Figure 7 shows the raw and depth-corrected spectra for each pixel. A double gaussian fit was applied to each histogram to disentangle the contributions from the photo-peak and the K-edge escape peak. The resolution at 1.275 MeV was evaluated as $R = 2.3548 * \delta/\mu$, where δ and μ were the standard deviation and mean parameters of the photo-peak gaussian component of the fit, respectively. Energy resolutions ranged between 3.4% and 4.0%. Figure 8 shows the raw and corrected energy distribution for events with drift times comprised between 3 and 6 μs for each pixel. This range of events was selected as it qualitatively exhibited the best performance in the 2D distributions in figure 6. The energy resolutions improved significantly and were 3.0%–3.3%.

4. Discussion

The distribution of intensity of Čerenkov fight measured in each event showed a series of peaks that in previous reports were identified as the number of detected Čerenkov photons per event (Ariño-Estrada et al 2018a, 2020). Based on the amplitude, which was offset-free as it was based on the differentiated signal of the SiPM, and relative distance between peaks, those identified in figure 4 are estimated to correspond to events with 3 through 8 detected Čerenkov photons. The simulation framework developed in the aforementioned reports estimated approximately 50 Čerenkov photons are generated for 1.275 MeV photoelectric depositions, with an average detection of ~10%–20% of the generated photons for TlBr crystals with similar dimensions, therefore, the results obtained in this study would match with those predictions. The signal-to-noise ratio of the Čerenkov signal is expected to improve with the detection of prompt-gammas with greater energy, based on the greater yield, and by using other photodetectors or photodetector settings. Besides, the Čerenkov signal has the potential to discern very effectively between gamma rays and other background particles in PRV such as electrons, protons, or neutrons.

The bands of the 1.275 MeV photopeak and the K-edge escape peak, at 1.190 MeV, in figure 6 were clear despite the presence of some noise in the background. Such noise could correspond to events with a strong charge induction (pixel) signal and an incorrect evaluation of the electron drift time. The incorrect evaluation of the drift time could be created by either a weak detected Čerenkov signal and/or a strong dark count pulse. No events were recorded near the anode (drift times close to 0) likely due to the presence of free charges that lead to charge recombination and severe loss of signal. However, this event region corresponds to drift times less than 1 μs, which corresponds to a detector slice of less than 0.5 mm.

The depth-correction applied in figure 7 improved the spectra significantly, which can be observed by the ratio between the photopeak and K-edge escape peak. The best performance was observed when events in the central part of the pixel were selected (3–6 μs), and energy resolutions between 3.0% and 3.3% at 1.275 MeV were measured. These are reasonable values considering the ratio of pixel pitch over detector thickness, 1.7/4 = 0.425. An improvement of energy resolution is expected for detectors with greater thickness, and thus smaller aspect ratio (Barret et al 1995). The shaping time of the spectroscopy amplifier, set to 8 μs in this study, could be slightly increased to prevent a potential ballistic deficit effect. Alternatively, full digital processing of the preamplifier output could be carried out as well with the same goal. None of these two approaches were feasible with the setup used in this work.

The band structures in figure 6 and the improvement of energy resolution by gating events with certain electron drift times do suggest this method can provide good DOI estimation. Although the positioning accuracy should be measured with a dedicated setup different from the one used in this study, it seems reasonable to expect the thickness of a detector like the one used in this work (4 mm) can be segmented in 4 parts to obtain, at least, 1 mm DOI accuracy.

DOI estimation and energy depth-correction can potentially be obtained in CCI detectors by reading out the cathode and applying either the CAR method or a cathode signal digitization. However, obtaining such estimates using the Čerenkov signal allows for a fully independent pixel readout and thus avoids overlap of signals from different events on the cathode, thus reducing the total effective dead time, which is crucial to ensure a high count rate capability with larger detector blocks.

An important future challenge for this detector concept is the system integration, as it requires two high-performance readouts, light and charge, with very different properties. However, this might be outweighed by its unique features like extreme accuracy, detection efficiency, or the potential to temporally resolve Compton kinematics.

5. Conclusion

This work is the first dedicated study of the energy resolution of a pixel CCI detector and how the estimation of electron drift time by combining the pixel and Čerenkov signals can be used for energy depth-correction. The energy resolution and evaluation of electron drift time achieved with the pixel CCI TlBr detector reasonably met the expectations for PRV in PGI. Given the timing resolution of a strip CCI TlBr detector for 511 keV photons was <400 ps, the timing performance for 1.275 MeV gammas is expected to be even better. Further evaluation of dead time and count rate capabilities of this detector as well as their performance in a cyclotron environment will be required. Preliminary data with CCI TlBr detectors already show an outstanding performance in energy, spatial, and timing resolution simultaneously, and suggest CCI TlBr detectors are excellent candidates to fit the needs of PRV in PGI.

Acknowledgments

This work has been supported by NIH grants R03 EB025533 (PI Ariño-Estrada) and R35 CA197608 (PI Cherry) and by an Innovative Developmental Award from the Academic Federation of the University of California, Davis (PI Ariño-Estrada).

References

Ariño-Estrada G, Mitchell GS, Kwon SI, Du J, Cirignano LJ, Shah KS and Cherry SR 2018a Towards time of flight PET with a semiconductor detector Phys. Med. Biol 63 04LT01

Ariño-Estrada G, Du J, Kim H, Cirignano LJ, Shah KS, Cherry SR and Mitchell GS 2018b Development of TlBr detectors for PET imaging Phys. Med. Biol 63 13NT04

Ariño-Estrada G, Mitchell GS, Kim H, Du J, Kwon SI, Cirignano LJ, Shah KS and Cherry SR 2019 First Cerenkov charge induction (CCI) TlBr detectors for TOF-PET and proton range verification Phys. Med. Biol 64 175001 [PubMed: 31344688]

Ariño-Estrada G, Roncali E, Selfridge A, Du J, Glodo J, Shah KS and Cherry SR 2020 Study of Čerenkov light in the semiconductors TlBr and TlC1 for TOF-PET IEEE Trans. Radiat. Plasma Med. Sci (10.1109/TRPMS.2020.3024032)

Barret HH, Eskin JD and Barber HB 1995 Charge transport in arrays of semiconductor gamma-ray detectors Phys. Rev. Lett 75 156–9 [PubMed: 10059139]

Berger MJ, Hubbell JH, Seltzer SM, Chang J, Coursey JS, Sukumar R, Zucker DS and Olsen K 2010 *XCOM: Photon Cross section Database* (version 1.5) National Institute of Standards and Technology, Gaithersburg, MD (10.18434/T48G6X)

Butterworth S 1930 On the theory of filter amplifiers Wireless Eng. 7 536–41

Cai L and Meng J-L 2013 Hybrid pixel-waveform CdTe/CZT detector for use in ultrahigh resolution MRI compatible SPECT system Nucl. Instrum. Methods Phys. Res. A 702 101–03

Churilov AV, Higgins WM, Ciampi G, Kim H, Cirignano LJ, Olschner F and Shah KS 2008 Purification crystal growth and detector performance of TlBr Proc. SPIE 7079 70790K

Durante M, Orecchia R and Loeffler JS 2017 Charged-particle therapy in cancer: clinical uses and future perspectives Nat. Rev. Clin. Oncol 14 483–95 [PubMed: 28290489]

Golnik C et al. 2014 Range assessment in particle therapy based on prompt γ-ray timing measurements Phys. Med. Biol 59 5399–422. [PubMed: 25157685]

He Z, Li W, G Knoll GF, Wehe DK, Berry JE and Stahle CM 1999 3D position sensitive CdZnTe gamma-ray spectrometers *Nucl. Instrum. Methods Phys. Res.* A 422 173–8

Hueso-González F, Rabe M, Ruggieri TA, Bortfeld T and Verburg JM 2018 A full-scale clinical prototype for proton range verification using prompt gamma-ray spectroscopy Phys. Med. Biol 63 185019 [PubMed: 30033938]

Krimmer J et al. 2015 Development of a Compton camera for medical applications based on silicon strip and scintillation detectors *Nucl. Instrum. Methods Phys. Res.* A 787 98–101

Lachish U 2001 Driving spectral resolution to the noise limit in semiconductor gamma detector arrays IEEE Trans. Nucl. Sci 48 520–3

Llosá G, Trovato M, Barrio J, Etxebeste A, Muñoz E, Lacasta C, Oliver JF, Rafecas M, Solaz C and Solevi P 2016 First images of a three-layer compton telescope prototype for treatment monitoring in hadron therapy Front. Oncol 6 14 [PubMed: 26870693]

Pausch G, Berthold J, Enghardt W, Römer K, Straessner A, Wagner A, Werner T and Kögler T 2018 Detection systems for range monitoring in proton therapy: needs and challenges *Nucl. Instrum. Methods Phys. Res.* A 954 161227

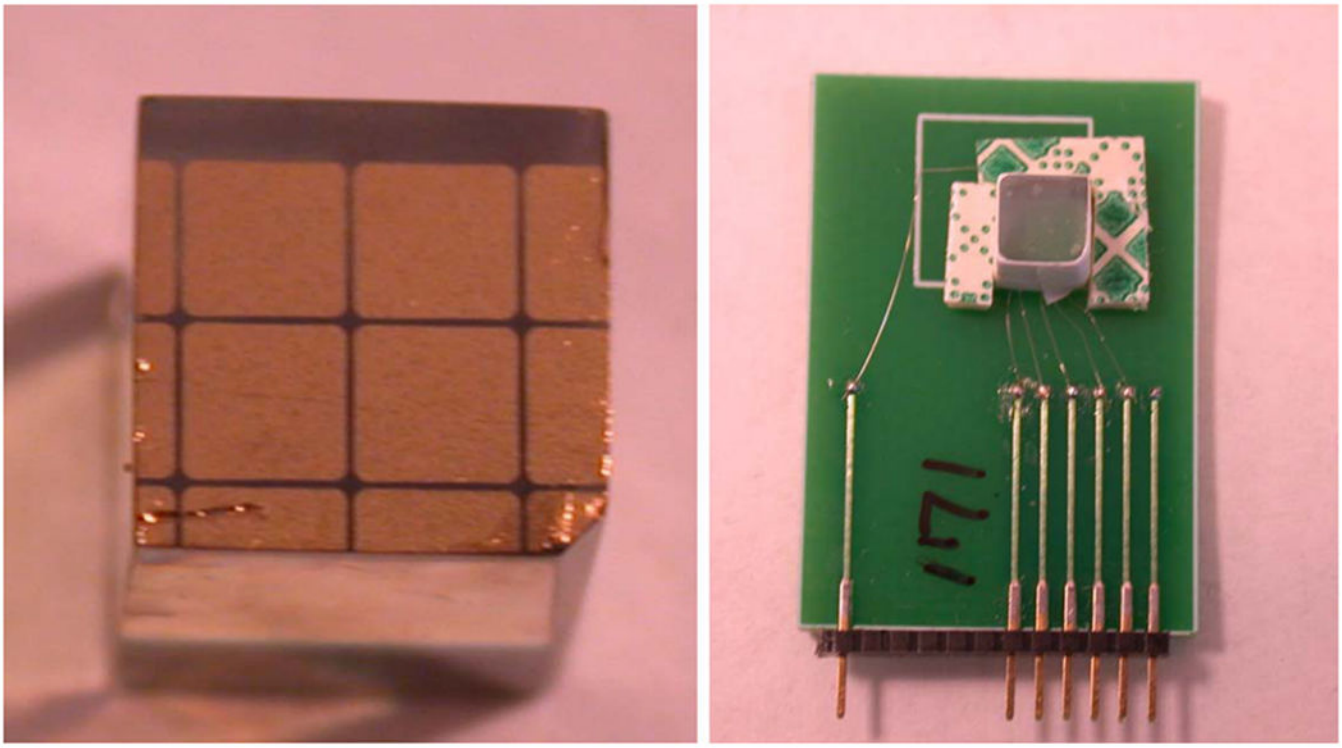

Figure 1.
(Left) Pixelated anode of the CCI detector used in this study. (Right) Same CCI TlBr detector mounted on a small PCB board.

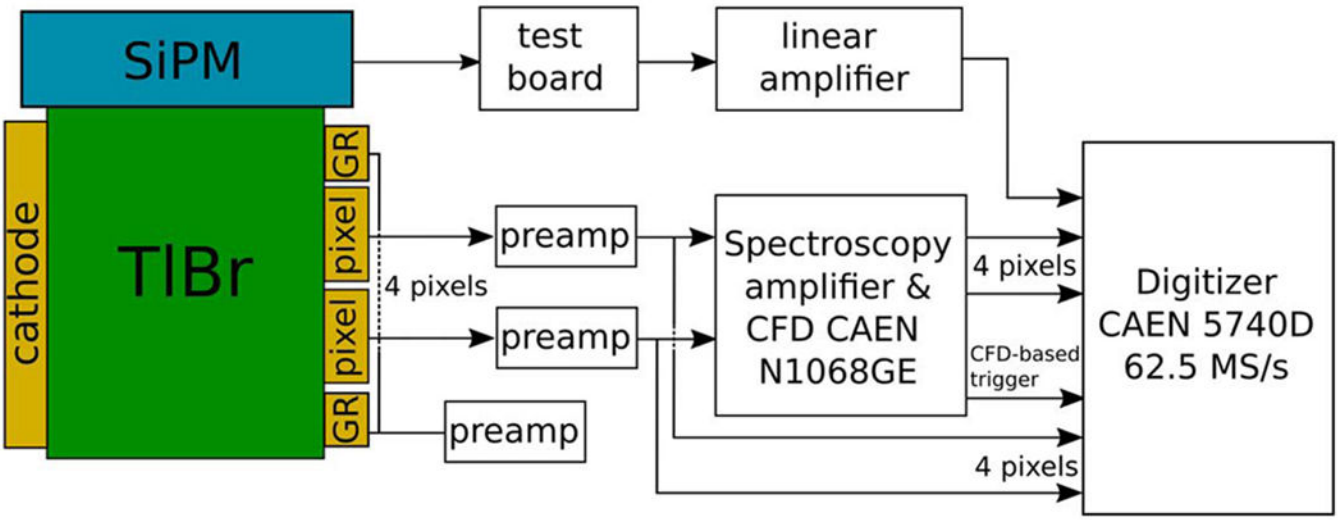

Figure 2.
Conceptual diagram of the setup used to readout the pixel CCI detector.

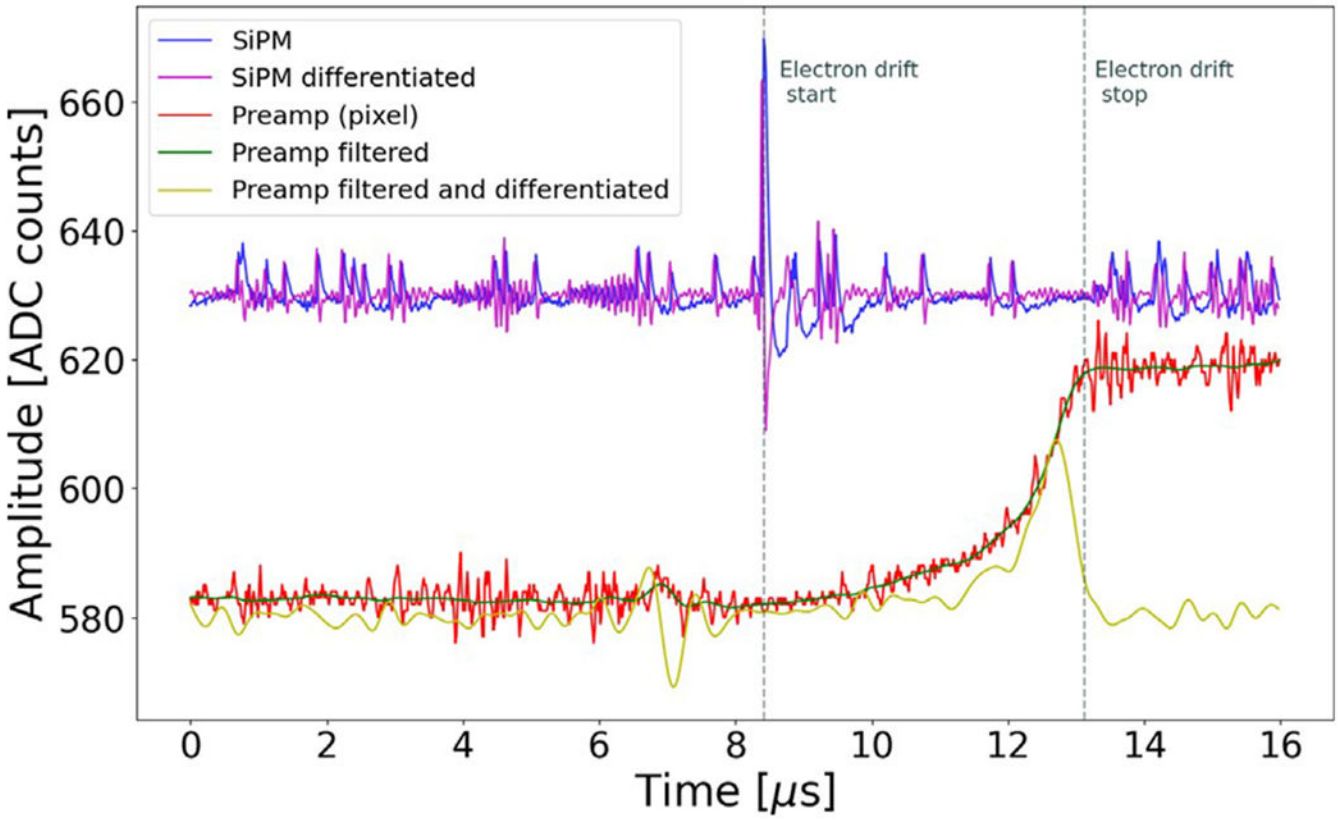

Figure 3.

SiPM, and preamplifier waveforms and their filtered and differentiated signals, of a representative event. The scale and offset of SiPM, SiPM differentiated, and the preamp filtered and differentiated signals were modified to facilitate visualization. The left and right vertical dashed lines correspond the start and end of the electron drift, respectively.

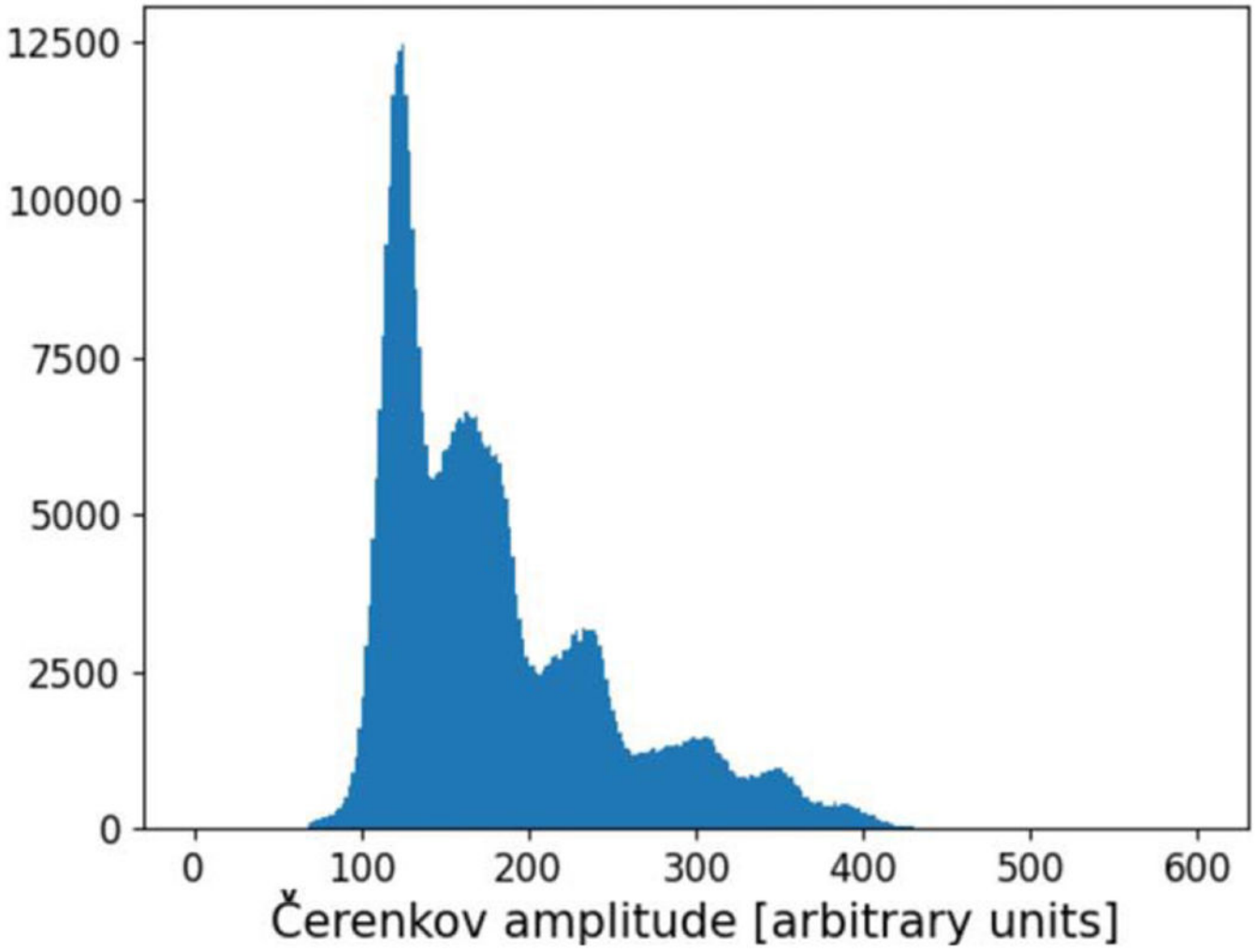

Figure 4.
Spectrum of the Cerenkov amplitude for all events registered with the pixel CCI detector.

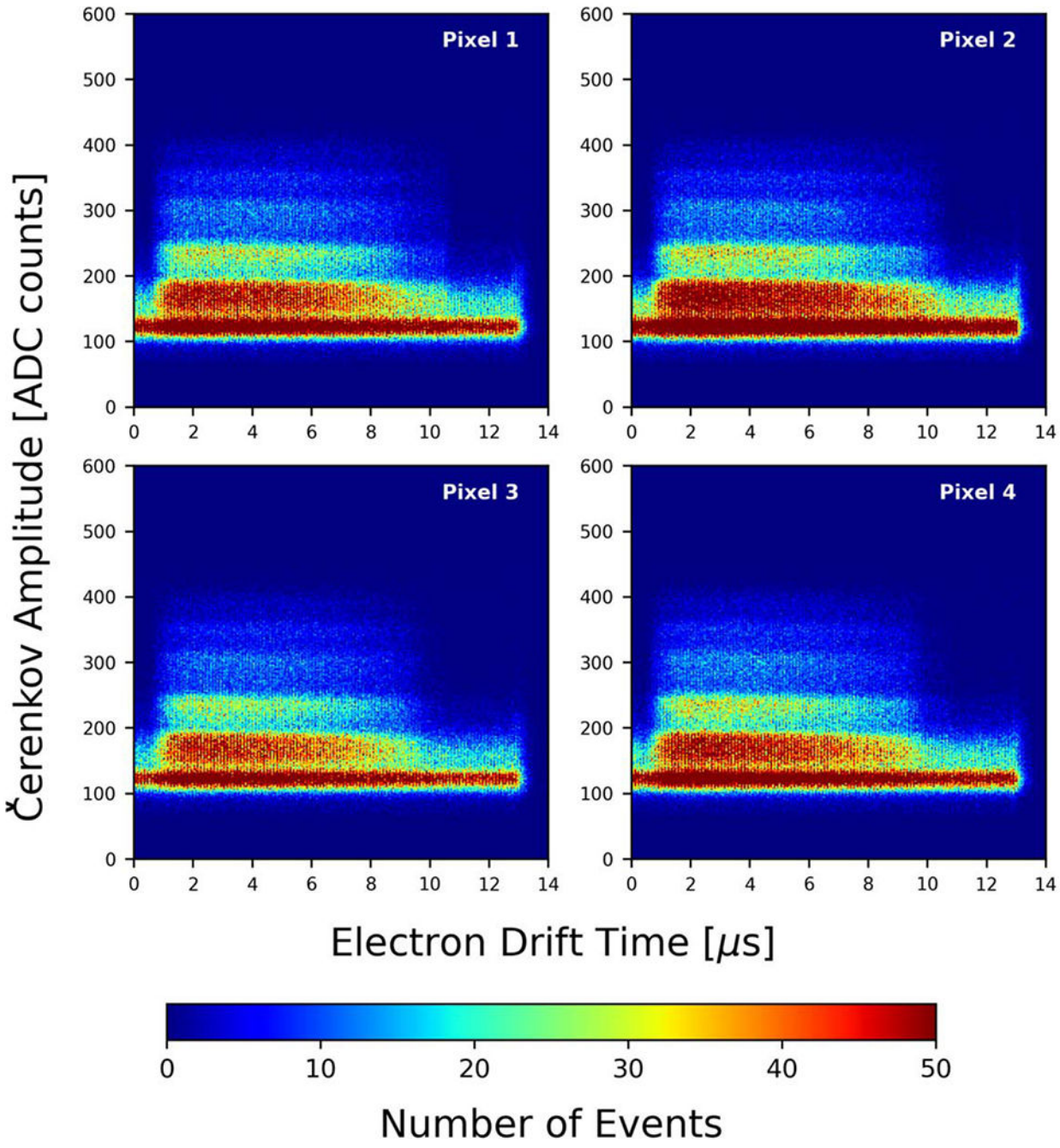

Figure 5.
Čerenkov amplitude versus electron drift time for events triggered by each of the four pixels.

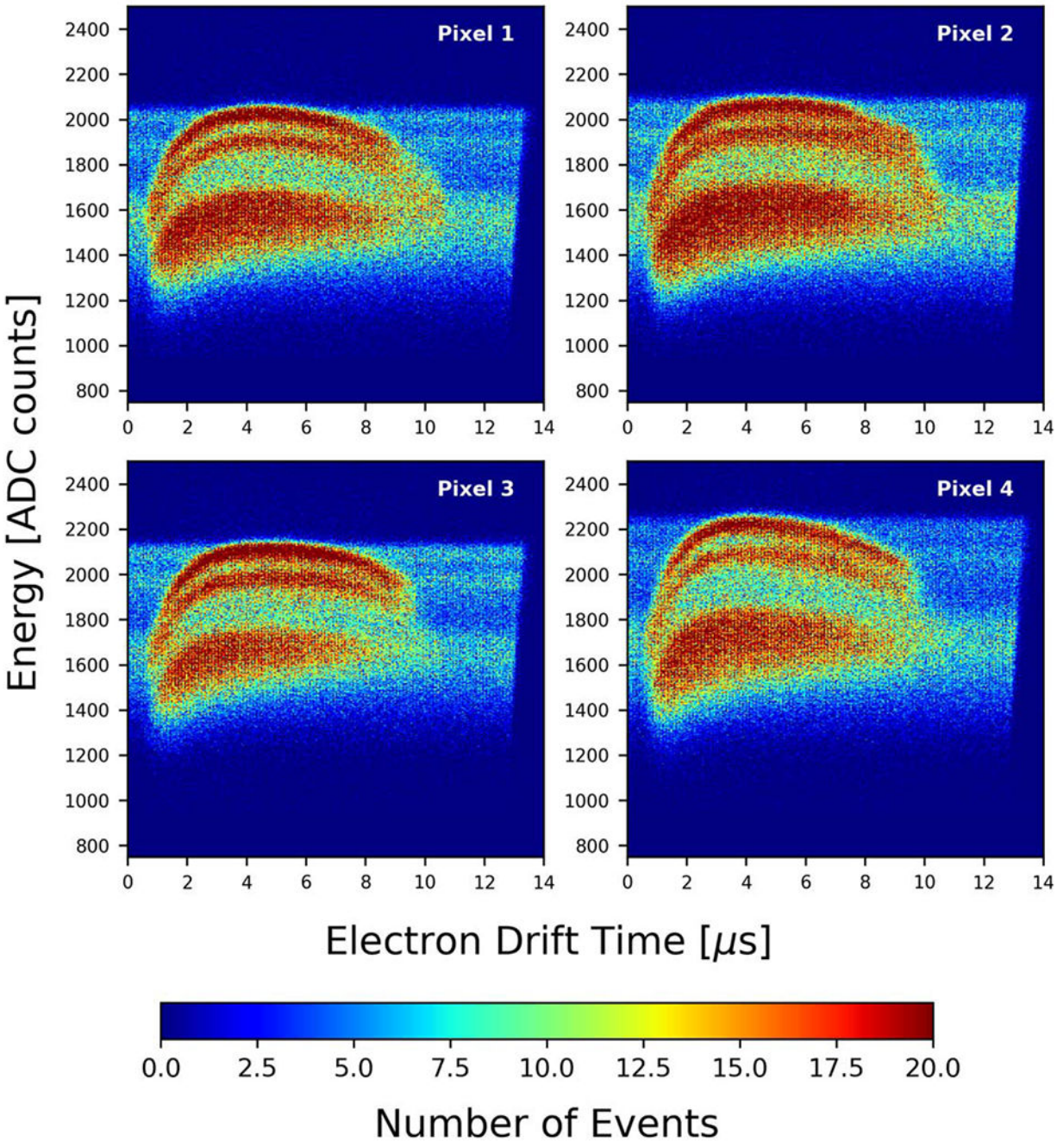

Figure 6.
Raw energy measurement versus drift time for events triggering in each pixel.

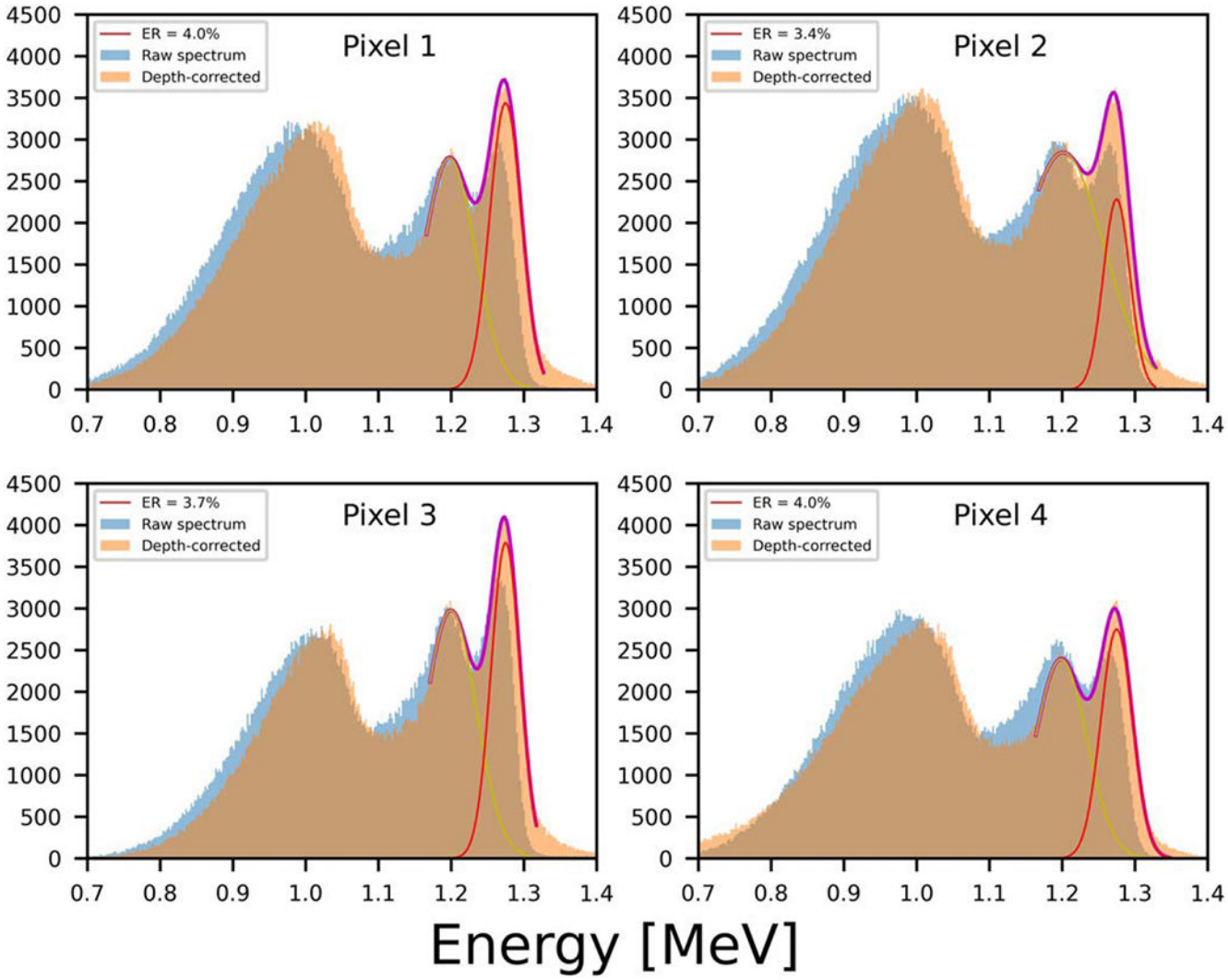

Figure 7.

Raw and depth-corrected spectroscopies for events triggering in each pixel and electron drift times between 1 and 9 μs. Purple lines represent a double gaussian fit and yellow and red ones the individual gaussian components.

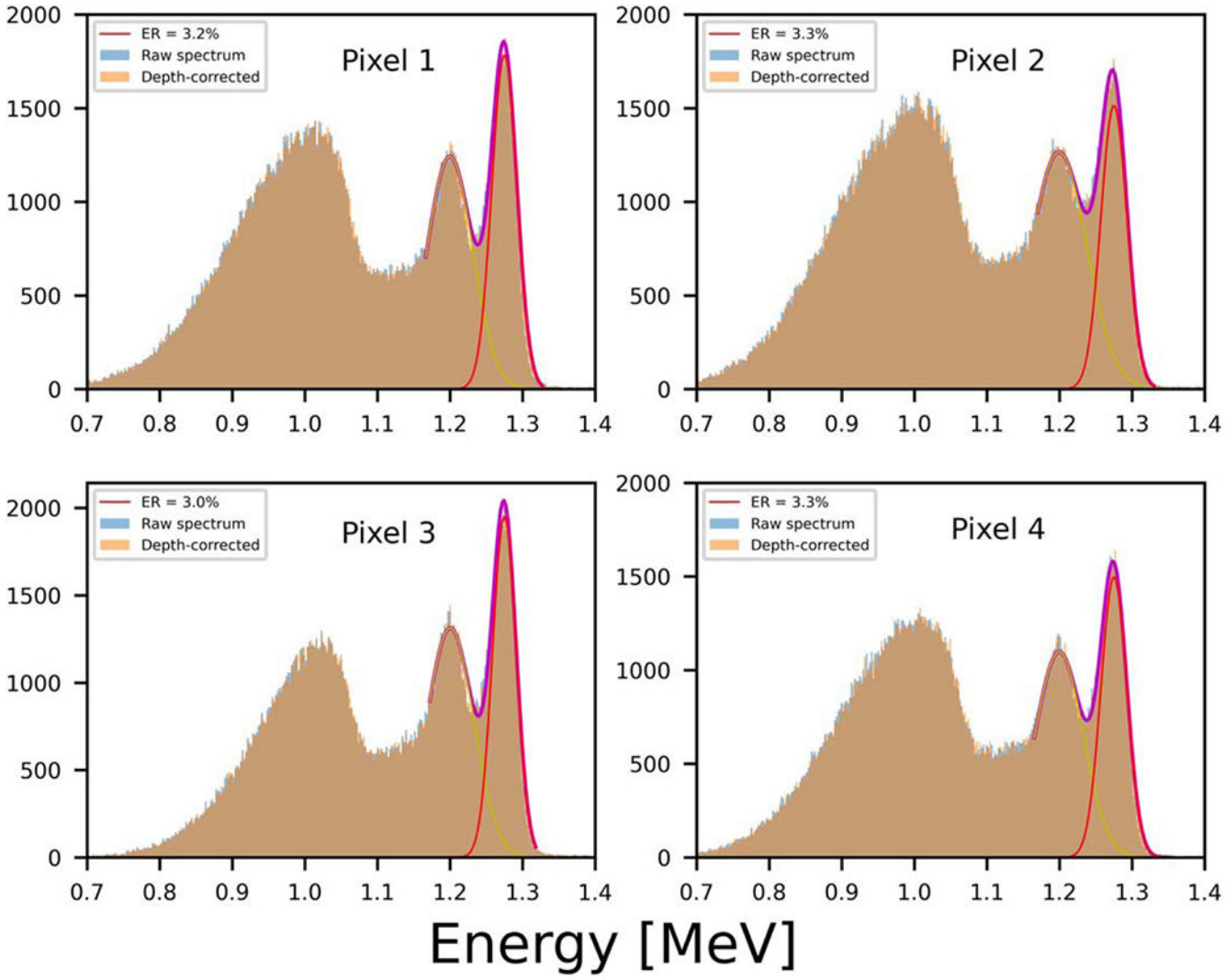

Figure 8.

Raw and depth-corrected spectra for events triggering each pixel using electron drift times between 3 and 6 μs. Purple lines represent a double gaussian fit and yellow and red ones the individual gaussian components.

Table 1.

Attenuation length [cm], including incoherent scattering, of several scintillation and semiconductor materials for gamma energies between 1 and 6 MeV. Data from Berger et al (2010).

Material	1 MeV	2 MeV	3 MeV	4 MeV	5 MeV	6 MeV
$LaBr_3$	3.42	4.82	5.46	5.74	5.83	5.83
$Cd_{0.9}Zn_{0.1}Te$	3.00	4.24	4.73	4.90	4.92	4.88
LSO	2.09	3.07	3.44	3.57	3.60	3.57
BGO	2.06	3.10	3.47	3.60	3.62	3.58
TlBr	1.98	2.98	3.29	3.36	3.34	3.28